Crystal Structure of a Conserved Ribosomal Protein-RNA Complex

Graeme L. Conn,[1] David E. Draper,[1]* Eaton E. Lattman,[2]* Apostolos G. Gittis[2]

The structure of a highly conserved complex between a 58-nucleotide domain of large subunit ribosomal RNA and the RNA-binding domain of ribosomal protein L11 has been solved at 2.8 angstrom resolution. It reveals a precisely folded RNA structure that is stabilized by extensive tertiary contacts and contains an unusually large core of stacked bases. A bulge loop base from one hairpin of the RNA is intercalated into the distorted major groove of another helix; the protein locks this tertiary interaction into place by binding to the intercalated base from the minor groove side. This direct interaction with a key ribosomal RNA tertiary interaction suggests that part of the role of L11 is to stabilize an unusual RNA fold within the ribosome.

The most important functional sites of ribosomes are associated with highly conserved domains of ribosomal RNAs (rRNAs); among these are the mRNA decoding site, the peptidyl transferase, and the site at which two elongation factors (EF-Tu and EF-G) alternately bind to position tRNA in the A site or to catalyze translocation of the mRNA (*1*). The latter site is associated with two extraordinarily well conserved regions of the large-subunit rRNA: the 17-nucleotide (nt) sarcin/ricin loop, and a 58-nt domain associated with ribosomal protein L11. Both of these RNA fragments are targeted by antibiotics, attesting to their functional importance. The 58-nt domain is particularly interesting: The sequence derived from *Escherichia coli* 23*S* rRNA adopts a specific, though marginally stable, tertiary structure that is further stabilized by L11 protein, itself highly conserved, or thiazole antibiotics (*2*, *3*). We report here the crystal structure of a complex between this 58-nt rRNA fragment and the 76-residue RNA binding domain of L11, at 2.8 Å resolution. The RNA is tightly folded by an extensive set of tertiary interactions that is locked into place by direct interaction of the protein with a key tertiary feature. This creates an unusually large interior of stacked bases and exposes a surface of conserved bases available for interaction with EF-G or antibiotic.

The RNA binding domain of *Bacillus stearothermophilus* L11 (L11-C76) was crystallized with an *E. coli* rRNA fragment containing a mutation that stabilizes tertiary structure (Fig. 1, A and B) (*4*), and its structure was determined by multiple wavelength anomalous diffraction (MAD) of a selenomethionyl derivative (*5*) (Table 1). Two complexes are present in the asymmetric unit and differ in only very minor ways. This suggests that crystal packing has not significantly perturbed the structure of the complex.

The RNA fold is stabilized in three locations by tertiary contacts between bases (Fig. 1, C and D). The junction loop is closed by helix B, which contains five canonical pairs and is terminated by a side-by-side G·A pair. From this point the RNA diverges into two helices. On one side, the reverse Watson-Crick U1082/A1086 base pair, previously deduced by comparative sequence analysis and compensatory base mutations (*6*), stacks onto the neighboring A helix. The three-base loop closed by U1082/A1086 forms a U-turn, a common motif for reversing chain direction (*7*). This turn places A1085 in position to hydrogen bond to G1055 in the minor groove of helix B. Both these bases are 99% conserved among sequences from the three phylogenetic domains (Bacteria, Archaea, and Eucarya) (*8*), suggesting their importance for stabilizing the structure. The other strand of helix B extends into helix C, which is interrupted by a two-base bulge loop. The first of these bases, A1088, is in the *syn* conformation and intercalates into helix A, where it forms a Hoogsteen pair with U1060; both of these bases are nearly invariant among the three phylogenetic domains. This pair is a key feature for protein recognition, discussed below. The second base of the bulge loop, A1089, lies in the same plane as A1090 with A1089 N3 hydrogen-bonded to A1090 N6 in what might be called an "A-A sidestep." Two more base triple interactions, involving bases from the helix A hairpin loop, stack on top of the A1089-A1090-U1101 triple (Fig. 2). An identical "A-A sidestep" has been seen in the "A platform" motif (*9*), where it also supports base triples but in a different way than seen here.

The structure of the helix C hairpin was previously solved by nuclear magnetic resonance (NMR) methods in the context of a 12- or 14-nt hairpin (*10*). It has essentially the same structure when part of the larger RNA domain, including a characteristic U-turn (Fig. 1, C and D). A third U-turn is found within the A helix hairpin. It places A1067 at the top of the turn, with G1068 stacked underneath and the rest of the hairpin loop extending deep within the structure to make contact with helix C. This is an unprecedented configuration for a hairpin loop, which depends on nonhelical torsion angles about the A1070 5′O–P, C4′–C5′, and 3′O–P bonds that unstack A1070 and reverse the chain direction. As a result, the highly conserved A1070 appears in a crevice between the A and C helices, where it stacks with A1061. It was previously thought that the U1061→A mutation stabilized RNA structure indirectly by preventing incorrect Watson-Crick pairing with A1077 (*11*). It now appears that this explanation is only partly correct, and that stacking with A1070 directly stabilizes the tertiary structure as well.

A pronounced feature of the overall RNA fold is the large interior core formed by stacked planes of bases. U1060, A1088, A1089, A1090, and U1101 all lie in a plane across the middle of the molecule, and additional planes of three or four bases are stacked above or below (Fig. 1D). This extensive stacking may account for the large heat capacity change of unfolding this RNA, which is larger than seen for any other nucleic acid and similar in magnitude to that seen for unfolding of protein hydrophobic cores (*2*). Two Mg^{2+} ions have been located within the interior core (Fig. 1D) and may correspond to two ions that strongly stabilize tertiary structure in solution (*12*).

The RNA contact surface of L11-C76 has previously been defined by NMR experiments to comprise the entire surface of helix 3, much of loop 2, and a central portion of loop 1 (*13*). Footprinting (*14*) and a compensatory mutation study (*15*) had suggested that the RNA contact surface would be centered about the conserved U1060 and A1077 nucleotides within helix A. These expectations are borne out by the crystal structure, which shows α-helix 3 against the minor groove surface of helix A (Fig. 3B). In the two known cases of α helices binding in an RNA major groove, the α helix is deep within the concave surface of the groove (*16*). In contrast, the helix A minor groove is relatively flat, in part due to distortions in the middle of the helix, and α-helix 3 is lying on its surface.

The unusual structure of helix A is a

[1]Department of Chemistry and [2]Department of Biophysics, Johns Hopkins University, Baltimore, MD 21218, USA.

*To whom correspondence should be addressed. E-mail: draper@jhunix.hcf.jhu.edu and lattman@jhu.edu

crucial factor in protein recognition. Insertion of A1088 into helix A requires that U1078 be turned out of the helix. U1078 then forms a stack with A1077 and G1062 across the width of the helix, sharply changing the direction of the helix axis (Fig. 3, A and B). On the opposite strand of the helix, A1061 is bulged and the backbone twists U1060 into a reverse polarity, placing the major groove edge of U1060 in the helix minor groove. A similar reversal of backbone polarity was seen in the Rev-RRE complex (*16*). The nearly invariant bases U1060, A1088, and G1059 are hydrogen-bonded to invariant parts of α-helix 3: The hydroxyl of Thr^{66}, which only varies to Ser, is hydrogen-bonded to O4 of U1060; the carbonyl of the invariant Gly^{65} bonds with N6 of A1088; and the Met^{62} carbonyl is bonded to N2 of G1059. The α carbon of Gly^{65} is packed against G1059 N2 and C1079 O2 and 2′O, which explains why no other amino acids are found at this position. Mutation of either Gly^{65} or Thr^{66} to alanine drastically reduces L11 binding affinity, demonstrating the importance of this set of hydrogen bonds (*17*). The invariance of these base–amino acid contacts accounts for the interchangability of L11 homologs between different organisms (*18*).

L11 dramatically stabilizes the entire tertiary structure of the 58-nt rRNA domain (*19*). The reason for this stabilization is now clear: By binding A1088 directly and stabilizing the helix A conformation that accommodates A1088, L11 locks a key tertiary interaction into place. Direct protein contact with a critical tertiary interaction has not been seen in other RNA-protein complexes and suggests a role for ribosomal proteins in stabilizing correct rRNA tertiary folds.

Besides Gly^{65} and Met^{62}, a third carbonyl-base hydrogen bond takes place between Ser^{69} and G1062; it is conserved in nearly all

Table 1: Summary of crystallographic statistics.

Data sets	Native	Selenomethionyl L11-C76–rRNA complex			
λ (Å)	1.13951	0.97914 (edge)	0.97871 (peak)	0.96675 (remote 1)	0.98557 (remote 2)
Resolution range (Å)	20–2.8	10–3.2	10–3.2	10–3.2	10–3.2
Measurements	89,078	72,499	72,879	72,186	72,579
Unique reflections	17,542	10,481	10,480	10,509	10,437
Completeness (%)*	94.5 (88.7)	88.3 (92.0)	88.3 (92.3)	88.7 (91.7)	88.2 (92.4)
$\langle I\rangle/\langle\sigma(I)\rangle$	23.3 (5.9)	38.0 (10.1)	37.9 (8.9)	40.5 (10.1)	32.4 (6.5)
$R_{sym}(I)$ (%)†	5.5 (24.0)	5.5 (23.8)	5.8 (26.6)	5.2 (22.3)	6.7 (35.6)
Phasing statistics (10–4.2 Å)					
Mean figure of merit		0.74 (0.61)			
R_{cullis} (dispersive)‡		–	0.77 (0.89)	0.60 (0.75)	0.71 (0.83)
R_{cullis} (anomalous)§		0.62 (0.81)	0.49 (0.70)	0.54 (0.76)	0.95 (0.97)
Phasing power‖		–	1.13 (0.54)	1.91 (1.16)	1.49 (1.10)
Refinement statistics					
R_{cryst} (R_{free}) (%)¶	24.0 (32.1)				
rmsd bond lengths (Å)	0.020				
rmsd bond angles (°)	2.642				
rmsd impropers (°)	4.118				

*Values in parentheses are statistics for the highest resolution bin. †$R_{sym}(I) = \Sigma_{hkl}\,|I_{hkl} - \langle I_{hkl}\rangle|/\Sigma_{hkl}I_{hkl}$, where I_{hkl} is the measured intensity of the reflection with indices *hkl*. ‡R_{cullis} (dispersive) $= \Sigma_{hkl}\|F_{PH} - F_P| - |F_H\|/\Sigma_{hkl}\|F_{PH}| - |F_H\|$ where $|F_P|$ and $|F_{PH}|$ are the native and derivative structure factor amplitudes and F_H the calculated heavy-atom structure factor amplitudes. §R_{cullis} (anomalous) is the ratio of the anomalous lack of closure and the anomalous difference. ‖Phasing power = rms f_h/E, where f_h is the heavy-atom structure factor amplitude and E is the residual lack of closure error. ¶$R = \Sigma_{hkl}\,\|F_{obs}| - |F_{calc}\|/\Sigma|F_{obs}|$, where $|F_{obs}|$ and $|F_{calc}|$ are the observed and calculated structure factor amplitudes for reflection *hkl*, applied to the work (R_{cryst}) and test (R_{free}) sets, respectively.

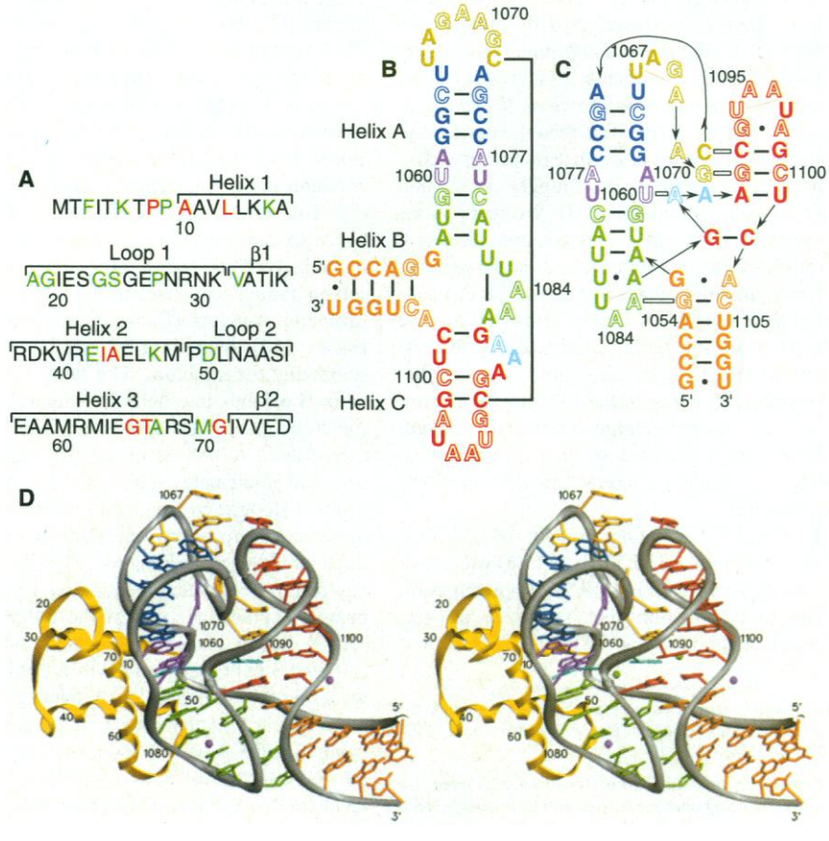

Fig. 1. Components of the L11-C76–rRNA complex. **(A)** Sequence of the *B. stearothermophilus* L11-C76 protein fragment (*19*, *25*). Secondary structure determined by NMR is marked, and colored residues are >80% conserved among 34 bacterial and plastid sequences (green) or additionally conserved in 22 archaeal and eukaryotic homologs (red). **(B)** Secondary structure of the 1051 to 1108 rRNA fragment of *E. coli* 23*S* rRNA as determined by comparative sequence analysis. Position 1061 has been mutated from U to A to stabilize tertiary structure. Bases in open typeface are conserved in greater than 97% of bacterial, archaeal, and eukaryotic rRNAs in a database of ~480 aligned sequences (*8*). The base triple C1072(C1092/G1099) was suggested by comparative sequence analysis and supported by compensatory mutations (*26*). **(C)** Secondary and tertiary structure of the same RNA. Color coding of bases is as in (B). Thin black lines with arrows indicate 5′→3′ direction of the backbone, black horizontal bars are Watson-Crick base pairs, dots are non–Watson-Crick base pairs, open horizontal bars are tertiary bonds between bases, and thin red lines indicate uridine N3 to phosphate hydrogen bonds characteristic of the U-turn motif. **(D)** Stereo view of the folded RNA and protein backbone. Mg^{2+} (green) and $Os(NH_3)_6^{3+}$ (magenta) are shown. The RNA bases in (B), (C), and (D) are color-coded for clarity. Abbreviations for the amino acid residues are as follows: A, Ala; D, Asp; E, Glu; F, Phe; G, Gly; I, Ile; K, Lys; L, Leu; M, Met; N, Asn; P, Pro; R, Arg; S, Ser; T, Thr; and V, Val.

bacteria. But in *Synechocystis* and plastid rRNAs, U1062/A1076 or C1062/U1076 substitutions have pyrimidine O2 in place of guanine N2. L11 sequences from these organisms have Asn in place of Ser[69], and this change has been shown to partially compensate for the deleterious effects of a U1062/A1076 substitution (*15*). On that basis, a specific contact between Ser[69] OH and G1062 N2 was proposed. Instead, Ser[69] OH bonds to both Thr[66] carbonyl and G1062 2′OH, and it is the Ser[69] carbonyl that interacts with G1062 N2. Whether an Asn[69] side chain bonds to U1062 or some other accommodation takes place in plastid ribosomes remains to be seen.

At either end of α-helix 3, loop 1 or loop 2 of L11-C76 closely approaches the helix A surface and makes a number of contacts, all but one of which are with the backbone (Fig. 3, A and B). Additional backbone contacts are made by α-helices 1 and 2 with the 5′ strand of helix A. Thus, L11 uses α-helix 3 to recognize conserved bases, and other parts of the protein to recognize the distorted shape of the helix A backbone.

The adjacent U1066 and U1094 U-turns expose the bases of A1067 and A1095 to solvent and bring them into proximity at one end of the RNA; the invariant base A1070 protrudes in a cleft between the two loops (Fig. 3C). A1095 and A1070 are conserved in more than 97% of sequences from the three phylogenetic domains, and position 1067 is always a purine (*8*). The conservation of these exposed bases is difficult to rationalize in terms of the RNA structure, which suggests that they are required for interactions with other components of the ribosome. Considerable biochemical evidence in fact points to these two loops as interaction sites for both thiostrepton and EF-G. A1067 and A1095 are associated with thiostrepton resistance in vivo or altered thiostrepton binding in vitro (*20*). Simultaneous interaction of thiostrepton with both loops—for example, by binding in the cleft between the loops—would account for its ability to stabilize the same (or very similar) rRNA tertiary structure as recognized by L11. The NH_2-terminal domain of L11 stimulates thiostrepton binding to the rRNA (*19*) and would be positioned nearby this cleft.

Thiostrepton inhibits the activity of EF-G (*21*), and this protein factor has also been localized to the U1066 and U1094 U-turns by various chemical methods (Fig. 3) (*22*). In direct binding assays, EF-G has been seen to interact with an 84-nt rRNA fragment containing the 58-nt sequence described here (*23*). Thus, direct contact of EF-G with either or both of the U1066 and U1094 U-turns seems likely. The bases protected by EF-G from chemical reaction are on the opposite face of the RNA from the proposed thiostrepton binding site (Fig. 3), suggesting that the factor and antibiotic bind at adjacent sites within this RNA.

As more ribosome functions are attributed to rRNA, it seems likely that a main function of ribosomal proteins is to stabilize required rRNA conformations. The fact that the *E. coli* rRNA fragment has a marginally stable tertiary structure in the absence of L11 supports this idea (*2*) and parallels observations that specific proteins trap active RNA conformations of some ribozymes (*24*). This look at a conserved protein-RNA complex from the ribosome will serve as a basis for more precise functional and structural analysis of the mechanisms by which L11, EF-G, and thiostrepton promote or inhibit ribosome activity.

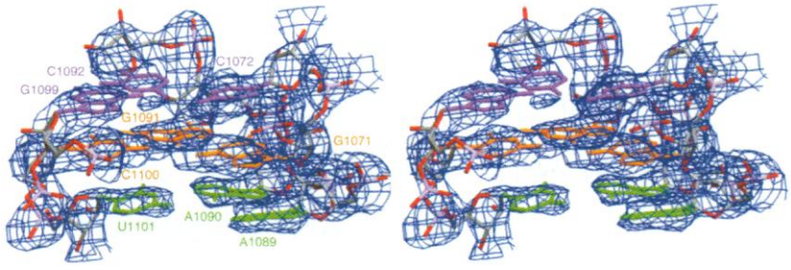

Fig. 2. Stereo view of the stack of three base triples. Shown is a $2F_o - F_c$ electron density map contoured at 1.0σ, calculated with the nine nucleotides in both RNA molecules omitted from the model (11% of the atoms in the asymmetric unit).

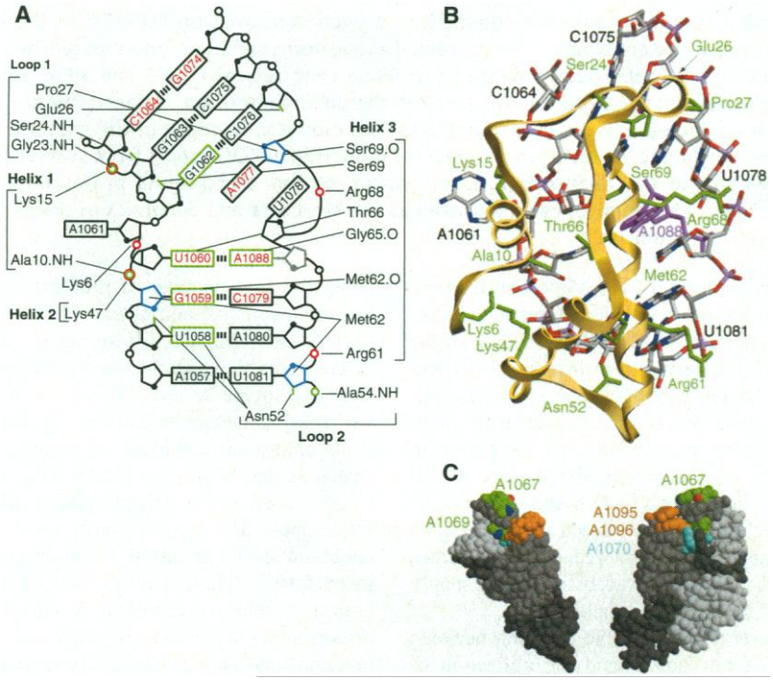

Fig. 3. Interactions of the RNA fragment. (**A**) Schematic of protein-RNA contacts. Bases lettered in red are ≥97% conserved among rRNA sequences. Protein residue contacts with RNA are coded by color: green, hydrogen bonds; red, electrostatic contact of basic residue with nonbridging phosphate oxygen; blue, nonpolar contact. Contacts are with amino acid side chain, unless noted as O (backbone carbonyl) or NH (backbone amide). Note that the backbone reverses direction at U1060, and that A1088 derives from another part of the RNA. (**B**) Backbone of L11-C76 on RNA surface. Many of the side chains indicated in (A) are shown. (**C**) Nucleotides potentially interacting with thiostrepton or EF-G. The RNA is shown as a space-filling model in two approximately orthogonal views. The sites of chemical protection by EF-G (N1; blue) and a 2′ OH where methylation confers thiostrepton resistance (red) are highlighted.

References and Notes

1. H. F. Noller, *Annu. Rev. Biochem.* **60**, 191 (1991).
2. L. G. Laing and D. E. Draper, *J. Mol. Biol.* **237**, 560 (1994).
3. Y. Xing and D. E. Draper, *ibid.* **246**, 319 (1995); D. E. Draper, Y. Xing, L. Laing, *ibid.* **249**, 231 (1995).
4. RNA was synthesized from linearized plasmid DNA encoding the 58-nt sequence with T7 RNA polymerase and L11-C76 expressed from pET11 vector with *E. coli* strain BL21 (DE3) as host (*26*). For MAD phasing, selenomethionyl-L11-C76 was produced by essentially the same procedure but with *E. coli* strain BL21 (B834-DE3) and minimal media containing seleno-

methionine [D. J. Leahy, W. A. Hendrickson, I. Aukhil, H. P. Erickson, *Science* **258**, 987 (1992)]. RNA and protein were mixed to equimolar concentration and crystals grown by sitting drop vapor diffusion from 50 mM sodium cacodylate (pH 6.5), 15% polyethylene glycol (PEG) 600, 80 mM $Mg(OAc)_2$, 100 mM KCl, and 0.2 mM $Co(NH_3)_6Cl_3$ at 37°C. The crystals typically had a size of 0.1 mm by 0.1 mm by 0.2 mm. The space group is $P4_32_12$ with unit cell dimensions $a = b = 150.68$ Å and $c = 63.84$ Å. The crystallographic asymmetric unit contains two complexes.

5. Diffraction data for selenomethionyl and native crystals were collected at beamline X4A, Brookhaven National Laboratories, Brookhaven, NY. Heavy-atom positions were determined with the program SOLVE [T. C. Terwilliger, *Methods Enzymol.* **276**, 530 (1997); www.solve.lanl.gov] and an experimental phase set generated with the program MLPHARE [Z. Otwinowsky, in *Isomorphous Replacement and Anomalous Scattering, Proceedings of the CCP4 Study Weekend*, W. Wolf, P. R. Evans, A. G. W. Leslie, Eds. (Science and Engineering Research Council Daresbury Laboratory, Warrington, UK, 1991), p. 80] in the resolution range 10.0 to 4.2 Å (Table 1). Experimental electron density maps were improved by solvent flattening with the SOLOMON procedure [J. P. Abrahams and A. G. W. Leslie, *Acta Crystallogr. D* **52**, 30 (1996)] and twofold noncrystallographic symmetry averaging. A model of L11-C76 (*13*) was fitted into the density with the Se-atom positions as a guide. A model of the RNA was built into the electron density map with the program O [T. A. Jones, J. Y. Zou, S. W. Cowan, M. Kjelgaard, *Acta Crystallogr. A* **47**, 110 (1991)]. During the initial stages of model building, the program SIGMAA [R. J. Read, *ibid.* **42**, 140 (1986)] was used to improve the electron density maps by phase recombination. Model refinement was performed with X-PLOR version 3.8 [A. T. Brünger, J. Kuriyan, M. Karplus, *Science* **235**, 458 (1987)]. A final round of model building and refinement (including grouped B factor refinement) against the native data set to 2.8 Å resolution was performed. The final crystallographic *R* factor is 24.0% against all reflections in the resolution range 8.0 to 2.8 Å (15,433 reflections) with an R_{free} [A. T. Brünger, *Nature* **355**, 472 (1992)] of 32.1% (1324 reflections) (Table 1). The model contains residues 6 to 72 of L11-C76 and all 58 nucleotides of the RNA. The two complexes in the asymmetric unit have a root-mean-square deviation (rmsd) of 0.60 Å on all protein and RNA backbone atoms (when aligned on Cα and phosphorus). The coordinates have been deposited in the RCSB Protein Databank (accession number 1QA6). Figures 1D, 2A, 2B, and 3B were generated with Setor [S. V. Evans, *J. Mol. Graphics* **11**, 134 (1993)] and Fig. 3C with Molscript [P. J. Kraulis, *J. Appl. Crystallogr.* **24**, 946 (1991)] and Raster3D [E. A. Merritt and D. J. Bacon, *Methods Enzymol.* **277**, 505 (1997)].
6. P. C. Ryan and D. E. Draper, *Proc. Natl. Acad. Sci. U.S.A.* **88**, 6308 (1991).
7. F. M. Jucker and A. Pardi, *RNA* **1**, 219 (1995).
8. R. Gutell, personal communication.
9. J. H. Cate *et al.*, *Science* **273**, 1696 (1996).
10. S. Huang, Y. X. Wang, D. E. Draper, *J. Mol. Biol.* **258**, 308 (1996); M. A. Fountain, M. J. Serra, T. R. Krugh, D. H. Turner, *Biochemistry* **35**, 6539 (1996).
11. M. Lu and D. E. Draper, *J. Mol. Biol.* **244**, 572 (1994).
12. Y. V. Bukhman and D. E. Draper, *ibid.* **274**, 1020 (1997). One Mg^{2+} ion sits between A1089 N1 and U1101 O4 and faces the 5′ phosphate of A1057; the other is close to O6 and N7 of G1059 and the 5′ phosphate of U1060. The ions are 3.6 to 4.6 Å from the specified ligands, implying that each ion remains completely hydrated. $Co(NH_3)_6^{3+}$ was present during crystallization, and in an effort to obtain heavy-atom derivatives, crystallization with $Os(NH_3)_6^{3+}$ was also tried. The Os atoms were only located at late stages of refinement in difference maps, and density at these same sites in $Co(NH_3)_6^{3+}$ crystals probably corresponds to that of Co. There are two Os atoms, located on the outside of the structure. One is between the major-groove edge of G1056 and the phosphate of U1101, and the other lies within hydrogen bonding distance of G1087 phosphate, U1081 O4, and U1082 O4 (Fig. 1D).
13. A. P. Hinck, *et al.*, *J. Mol. Biol.* **274**, 101 (1997).
14. G. Rosendahl and S. Douthwaite, *ibid.* **234**, 1013 (1993).
15. D. GuhaThakurta and D. E. Draper, *Biochemistry* **38**, 3633 (1999).
16. J. L. Battiste, *et al.*, *Science* **273**, 1547 (1996); P. Legault, J. Li, J. Mogridge, L. E. Kay, J. Greenblatt, *Cell* **93**, 289 (1998).
17. Y. Xing, D. GuhaThakurta, D. E. Draper, *Nature Struct. Biol.* **4**, 24 (1997).
18. T. T. A. L. El-Baradi *et al.*, *J. Mol. Biol.* **195**, 909 (1987); J. Thompson, W. Musters, E. Cundliffe, A. E. Dahlberg, *Eur. J. Biochem.* **12**, 1499 (1993).
19. Y. Xing and D. E. Draper, *Biochemistry* **35**, 1581 (1996).
20. E. Cundliffe and J. Thompson, *Nature* **278**, 859 (1979); H. Hummel and A. Böck, *Biochemie* **69**, 857 (1987); G. Rosendahl and S. Douthwaite, *Nucleic Acids Res.* **22**, 357 (1994).
21. E. Cundliffe, in *Structure, Function, and Genetics of Ribosomes*, B. Hardesty and G. Kramer, Eds. (Springer-Verlag, New York, 1986), p. 586.
22. K. S. Wilson and H. F. Noller, *Cell* **92**, 131 (1998).
23. A. Munishkin and I. G. Wool, *Proc. Natl. Acad. Sci. U.S.A.* **94**, 12280 (1997).
24. K. M. Weeks and T. R. Cech, *Science* **271**, 345 (1996); V. Gopalan, A. D. Baxevanis, D. Landsman, S. Altman, *J. Mol. Biol.* **267**, 765 (1997).
25. Protein residues are numbered from the initiator methionine of the L11-C76 protein fragment. Thr^2 of L11-C76 corresponds to Thr^{59} of the *B. stearothermophilus* sequence currently in the sequence databases, although that sequence is missing up to nine residues from the NH_2-terminus.
26. G. L. Conn, R. R. Gutell, D. E. Draper, *Biochemistry* **37**, 11980 (1998).
27. Supported by NIH R37 GM29048 (D.E.D.) and the Wellcome Trust, UK (G.L.C.). We are grateful to C. Ogata, D. Cook, C. Foster, D. Karp, and C. Garvie for assistance with data collection and processing. We also thank D. Leahy and M. Bianchet for helpful discussions.

6 April 1999; accepted 16 April 1999

Long-Term Discrepancy Between Food Supply and Demand in the Deep Eastern North Pacific

Kenneth L. Smith Jr.[1*] and Ronald S. Kaufmann[2]

A 7-year study of food supply [sinking particulate organic carbon (POC)] and food demand [sediment community oxygen consumption (SCOC)] in the abyssal eastern North Pacific revealed a long-term deficit in food supply. The POC:SCOC ratio decreased by 52 to 59 percent between 1989 and 1996. A possible explanation for this trend is the documented sea surface temperature increase and concomitant plankton biomass decrease in the eastern North Pacific, resulting in an apparent reduction in POC export from surface waters to the deep ocean. Continuation of this trend could profoundly impact geochemical cycling as well as the structure and dynamics of deep-sea communities.

Recent long-term increases in sea surface and upper water column temperatures in the eastern North Pacific have led to shoaling of the mixed layer, resulting in a reduced nutrient supply to the euphotic zone (*1*). Concomitantly, there has been a decline in primary productivity accompanied by decreases in zooplankton and seabird abundances as well as kelp production (*1–4*). Deep-sea communities rely on food produced in the euphotic zone, and a long-term reduction in surface productivity could severely impact the supply of food to the deep ocean.

Efforts to examine the coupling between pelagic food sources and the utilization of this food by deep-sea communities have been hampered by a number of problems. These include qualitative and quantitative diversity in food sources, the diffuse nature of the mechanisms by which this food is transported from its source to the abyssal ocean, and variability in metabolic demands by deep-sea communities on a variety of temporal and spatial scales. Short-term studies of trophic coupling between a pelagic (water column) food supply and benthic (surface sediment) communities in the deep ocean have been inconclusive. These studies have revealed both acceptable agreement and unexplained discrepancies, depending on geographic location and time of year (*5–7*). These inconsistencies have prompted long-term studies of temporal variation in the flux of sinking particulate organic carbon (POC), as a measure of food supply reaching the sea floor from the overlying water column, and sediment community oxygen consumption (SCOC), as an estimate of metabolic demand for organic carbon (*8*, *9*).

A 7-year study was conducted to examine

[1]Marine Biology Research Division, Scripps Institution of Oceanography, University of California, San Diego, La Jolla, CA 92093–0202, USA. [2]Marine and Environmental Studies Program, University of San Diego, 5998 Alcalá Park, San Diego, CA 92110–2492, USA.

*To whom correspondence should be addressed. E-mail: ksmith@ucsd.edu